Earth and Planetary Science Letters 277 (2009) 223–235

Contents lists available at ScienceDirect

Earth and Planetary Science Letters

journal homepage: www.elsevier.com/locate/epsl

Reductive diagenesis, magnetite dissolution, greigite growth and paleomagnetic smoothing in marine sediments: A new view

Christopher J. Rowan *, Andrew P. Roberts, Thomas Broadbent [1]

National Oceanography Centre, University of Southampton, European Way, Southampton SO14 3ZH, United Kingdom

ARTICLE INFO

Article history:
Received 21 April 2008
Received in revised form 15 October 2008
Accepted 18 October 2008
Available online 6 December 2008

Editor: M.L. Delaney

Keywords:
sediment diagenesis
sulfate reduction
magnetite dissolution
greigite
superparamagnetism
hysteresis

ABSTRACT

In many anoxic sedimentary environments, the onset of sulfate reduction, and pyritization of detrital iron-bearing minerals, leads to a precipitous decline in magnetic mineral concentration during early diagenesis. The usefulness of the surviving paleomagnetic record in such environments is usually argued to depend on how much of the primary detrital magnetic assemblage survives diagenetic dissolution. Detailed rock magnetic and electron microscope analyses of rapidly deposited (~7 cm/kyr) latest Pleistocene–Holocene sediments from the continental margins of Oman (22°22.4′N, 60°08.0′E) and northern California (38°24.8′N, 123°58.2′W) demonstrate that pyritization during early diagenesis also leads to the progressive down-core growth of the ferrimagnetic iron sulfide greigite. Greigite growth begins with nucleation of large concentrations of superparamagnetic (SP) nanoparticles at the inferred position of the sulfate–methane transition, which can explain the apparently paradoxical suggestion that diagenetically reduced sediments contain enhanced concentrations of SP particles. Looping of hysteresis parameters on a "Day" plot records the dissolution of single domain (SD) (titano-)magnetite and the formation of SP greigite, which then slowly and progressively grows through its SD blocking volume and acquires a stable paleomagnetic signal. This looping trend is also evident in data from several published records (Oregon margin, Korea Strait, Japan Sea, Niger Fan, Argentine margin, and the Ontong–Java Plateau), indicating that these processes may be widespread in reducing environments. Our observations have profound implications for paleomagnetic records from sulfate-reducing environments. The paleomagnetic signal recorded by greigite is offset from the age of the surrounding sediments by 10's of kyr, and ongoing growth of greigite at depth results in smoothing of the recorded signal over intervals of 10's to 100's of kyr. We therefore expect the presence of greigite to compromise paleomagnetic records in a wide range of settings that have undergone reductive diagenesis.

1. Introduction

The widespread occurrence of magnetically stable greigite (Fe_3S_4) in rapidly deposited marine sediments is now well-established (Tric et al., 1991; Horng et al., 1992; Roberts and Turner, 1993; Florindo and Sagnotti, 1995; Horng et al., 1998; Sagnotti and Winkler, 1999; Jiang et al., 2001; Kao et al., 2004; Roberts et al., 2005; Rowan and Roberts, 2006; Larrasoaña et al., 2007; Vasiliev et al., 2007). Conventional views of steady-state diagenesis (e.g., Berner, 1984) predict that in active depositional settings, iron sulfide formation should be restricted to the top of the anoxic zone, where detrital iron-bearing minerals, including magnetite, react with hydrogen sulfide (H_2S) produced during bacterially-mediated anaerobic reduction of sulfate to produce pyrite (FeS_2) (Karlin and Levi, 1983, 1985; Canfield and Berner, 1987; Karlin, 1990a,b). Greigite is an intermediate phase in this reaction (Berner, 1984; Wilkin and Barnes, 1997; Hunger and Benning, 2007), and can be preserved if the supply of organic carbon, and hence H_2S, is limited in the presence of abundant reactive iron (Kao et al., 2004). The absence of pore water sulfate deeper in the sediment column should inhibit pyritization. Therefore, according to steady-state diagenetic models, any magnetically stable greigite found in marine sediments should have formed in a single brief period shortly after deposition, offsetting and moderately smoothing the recorded magnetic signal in a manner analogous to the smoothed post-depositional remanent magnetizations produced just below a bioturbated surface layer. It was therefore often assumed in early paleomagnetic studies of greigite-bearing sediments that the greigite had an early diagenetic origin, and that it accurately recorded the geomagnetic field close to the time of deposition (e.g., Tric et al., 1991; Roberts and Turner, 1993).

In reality, greigite-bearing sedimentary rocks often have complex paleomagnetic signatures, consistent with the growth of authigenic iron sulfides over far greater timescales. Such behavior includes

* Corresponding author. Now at School of Geosciences, The University of Edinburgh, West Mains Road, Edinburgh, EH9 3JW, United Kingdom.
E-mail address: c.j.rowan@gmail.com (C.J. Rowan).
[1] Now at School of Ocean Sciences, University of Wales Bangor, Menai Bridge, Anglesey LL59 5AB, United Kingdom.

0012-821X/$ – see front matter © 2008 Published by Elsevier B.V.
doi:10.1016/j.epsl.2008.10.016

contradictory polarities within the same stratigraphic horizon (Horng et al., 1998; Jiang et al., 2001; Roberts et al., 2005); spurious magnetic polarity patterns that are inconsistent with independent age controls (Florindo and Sagnotti, 1995; Rowan and Roberts, 2005; Sagnotti et al., 2005); and pervasive remagnetization of entire regions several million years after deposition (Rowan and Roberts, 2006, 2008). Even when greigite-bearing sequences appear to contain detailed records of geomagnetic polarity transitions (Tric et al., 1991), scanning electron microscope (SEM) observations of preserved iron sulfides routinely indicate multiple generations of authigenic greigite growth (e.g., Roberts et al., 2005). In active depositional environments, greigite formation has been documented tens of meters below the sediment–water interface (Liu et al., 2004; Schwehr et al., 2006), which further suggests that even during early diagenesis, the processes that control greigite growth and preservation may operate over much longer timescales than is often assumed.

Rapidly deposited marine sediments are frequently targeted for high-resolution paleomagnetic and environmental magnetic studies. However, in sequences where bacterial sulfate reduction has resulted in dissolution of the primary magnetic assemblage, late authigenic growth of even small amounts of greigite could severely compromise the magnetic record. In this paper, we present results of detailed rock magnetic and SEM studies of sediment cores from the Oman and northern California margins (Fig. 1), which provide important new constraints on the patterns and timing of magnetic iron sulfide growth in active depositional settings. Our work also highlights the limitations of greigite as a recorder of short-term environmental and geomagnetic variations.

2. Materials and methods

2.1. Oman margin: core CD143-55705

CD143-55705 is a 10.63 m piston core recovered from a water depth of 2193 m on the Oman margin in the northwestern Arabian Sea (22°22.4′N, 60°08.0′E) (Fig. 1) in November 2002 (Jacobs, 2003). In this region, the strong southwesterly winds of the summer monsoon drive upwelling of nutrient-rich waters, which results in high primary productivity of ~200 g C m^{-2} yr^{-1} (Nair et al., 1989). Export of organic carbon (C_{org}) to the sea-floor is also high, with sediments typically having C_{org} values of 1–2% (Sirocko et al., 2000). Magnetic mineral diagenesis has been widely documented in organic-rich sediments from the Arabian Sea (e.g., Bloemendal et al., 1992, 1993; Hounslow and Maher, 1999). The studied core is composed of homogeneous, light grey-green to green-brown hemipelagic mud, with few sedimentological features. Foraminiferal $\delta^{18}O$ measurements indicate that Stage 6 of the marine isotope record (130–195 ka) is reached at a depth of 7.54 m, and that the Holocene sedimentation rate was 6–8 cm/kyr (Bryson, 2006). U-channel samples (4 cm^2 cross-section; Weeks et al., 1993) were collected from the middle of each ~1.5 m core section and analysed at the National Oceanography Centre, Southampton (NOCS). Low-field volume magnetic susceptibility (κ) was measured at 1-cm intervals on a track system incorporating a Bartington Instruments MS2C loop sensor, prior to measurements at 1-cm intervals of the natural remanent magnetization (NRM), anhysteretic remanent magnetization (ARM), and isothermal remanent magnetization (IRM) on a 2-G Enterprises cryogenic magnetometer situated in a magnetically shielded laboratory. The following measurement sequence was used.

(1) The NRM was measured after progressive stepwise alternating field (AF) demagnetization (at 5 mT steps to 30 mT, then at 40, 50, 60, and 80 mT).
(2) An ARM was imparted by applying a 90 mT AF in the presence of an axial 0.05 mT bias field. The ARM was then measured and progressively AF demagnetized (at 5 mT steps to 30 mT, then at 40 and 60 mT).
(3) An IRM was imparted to the u-channel samples by applying a 900 mT direct field (IRM_{900}) with a 2-G Enterprises pulse magnetizer, then measured and progressively AF demagnetized (at 0, 10, 20, 25, 30, 40, 60 and 90 mT).
(4) A second IRM_{900} was imparted prior to applying a 300 mT backfield and measuring the IRM_{-300}, to allow calculation of the *S*-ratio ($-IRM_{-300}/IRM_{900}$) and the 'hard IRM' ($HIRM=(IRM_{900}-IRM_{-300})/2$).

Magnetic hysteresis properties of air-dried, ~1 cm^3 sub-samples, taken at approximately 20 cm stratigraphic intervals with a ceramic knife, were then measured on a Princeton Measurements Corporation vibrating sample magnetometer. Saturation magnetization, M_s, saturation remanent magnetization, M_r, and coercive force, B_c, were determined from hysteresis loops (maximum applied field of 0.5 T), following a paramagnetic slope correction. The coercivity of remanence, B_{cr}, was determined from back-field remanence curves. 140 first-order reversal curves (FORCs) (Pike et al., 1999; Roberts et al.,

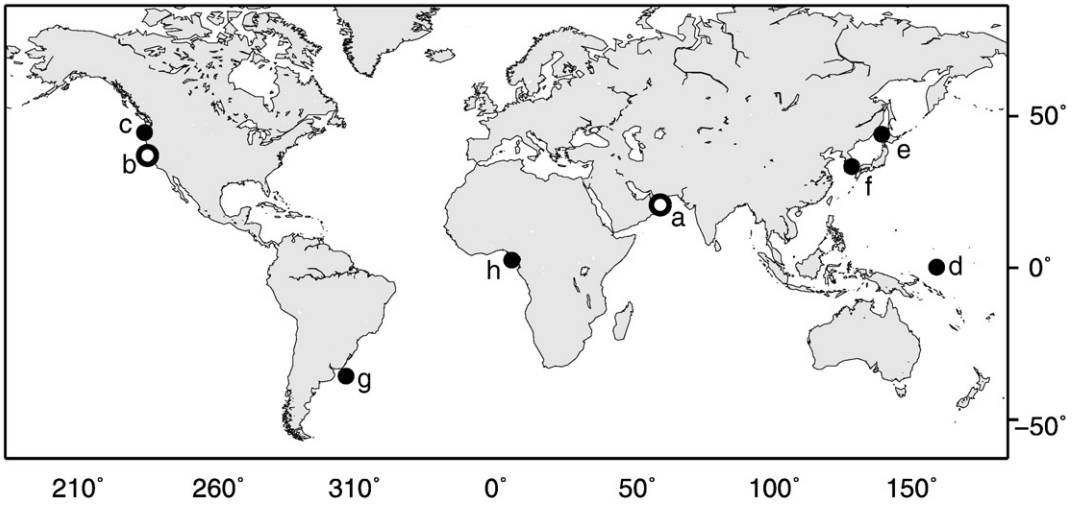

Fig. 1. Locations of the cores analysed in this study (open circles) and previously published records (closed circles) that are discussed in this paper. a. Oman margin (core CD143-55705); b. northern California margin (core L13-81-G138); c. Oregon margin (Karlin, 1990a); d. Ontong–Java Plateau (Tarduno, 1994, 1995); e. Japan Sea (Yamazaki et al., 2003); f. Korean Strait (Liu et al., 2004); g. Argentine margin (Garming et al., 2005); and h. Niger Fan (Dillon and Bleil, 2006).

2000), with a field spacing of 1.85 mT, averaging time of 250 ms, and a 0.5 T saturating field, were also measured; FORC distributions were calculated using the FORCinel package (Harrison and Feinberg, 2008) with a smoothing factor (SF) of 5.

Finally, resin-impregnated polished sections were made from selected sub-samples and examined on a LEO 1450VP SEM, operated at 10–20 keV with an acceleration voltage of 17–20 pA. A Princeton Gamma Tech (IMIX-PTS) X-ray energy dispersive spectrometer (EDS), calibrated with a pyrite standard, was used for elemental analyses of iron sulfide phases. Numerous studies have demonstrated that different phases such as greigite and pyrite can be distinguished by their distinctive iron to sulfur ratios (Fe/S = 0.75 and = 0.5, respectively) (Jiang et al., 2001; Roberts and Weaver, 2005; Rowan and Roberts, 2005; Sagnotti et al., 2005; Rowan and Roberts, 2006).

2.2. Northern California margin: core L13-81-G138

L13-81-G138 is a ~4.5 m gravity core recovered by the United States Geological Survey from a water depth of 2531 m on the northern California margin (38°24.8′N, 123°58.2′W) (Fig. 1). This region has high summer productivity due to strong upwelling driven by the south-flowing California Current, which represents the eastern limb of the North Pacific gyre. The large sediment supply from the North American continent also provides a significant amount of organic carbon to marginal sediments; C_{org} reaches values of ~2.8% at the top of core L13-81-G138 (Dean et al., 1994), 30–40% of which is of terrestrial origin (Gardner et al., 1997). The studied core comes from a location between the Oregon margin to the north and the "California Continental borderland" to the south. These localities were analysed in what are now classic studies of magnetic mineral diagenesis (Karlin and Levi, 1983, 1985; Karlin, 1990a,b; Leslie et al., 1990a,b). AMS ^{14}C dating has established a calendar age of 31.184 ka for material from a depth of 3.98 m, and a Holocene sedimentation rate of 6–7 cm/kyr (Gardner et al., 1997).

Paleomagnetic analysis of 91 discrete samples (8 cm^3 volume), collected at an average stratigraphic spacing of 5 cm, was conducted in the paleomagnetic laboratory at the University of California, Davis, in 1993. κ and NRM were measured for all samples, but detailed stepwise AF demagnetization (5 mT steps to 30 mT) was only performed on the 30 samples collected from the core above a depth of 1.5 m, and for every tenth sample below this depth (average stratigraphic spacing ~45 cm). Measurement of an ARM (imparted with a 0.05 mT dc bias field in a 100 mT AF, followed by stepwise AF demagnetization at 5 mT steps to 30 mT, then at 10 mT steps to 60 mT) was performed for every tenth sample from the core. Hysteresis parameters and IRM_{900} were measured for every sample in the uppermost 0.5 m of the core, and for every second sample below this depth. FORC measurements were made for every sample at NOCS in 2006 using the procedures described above for core CD143-55705.

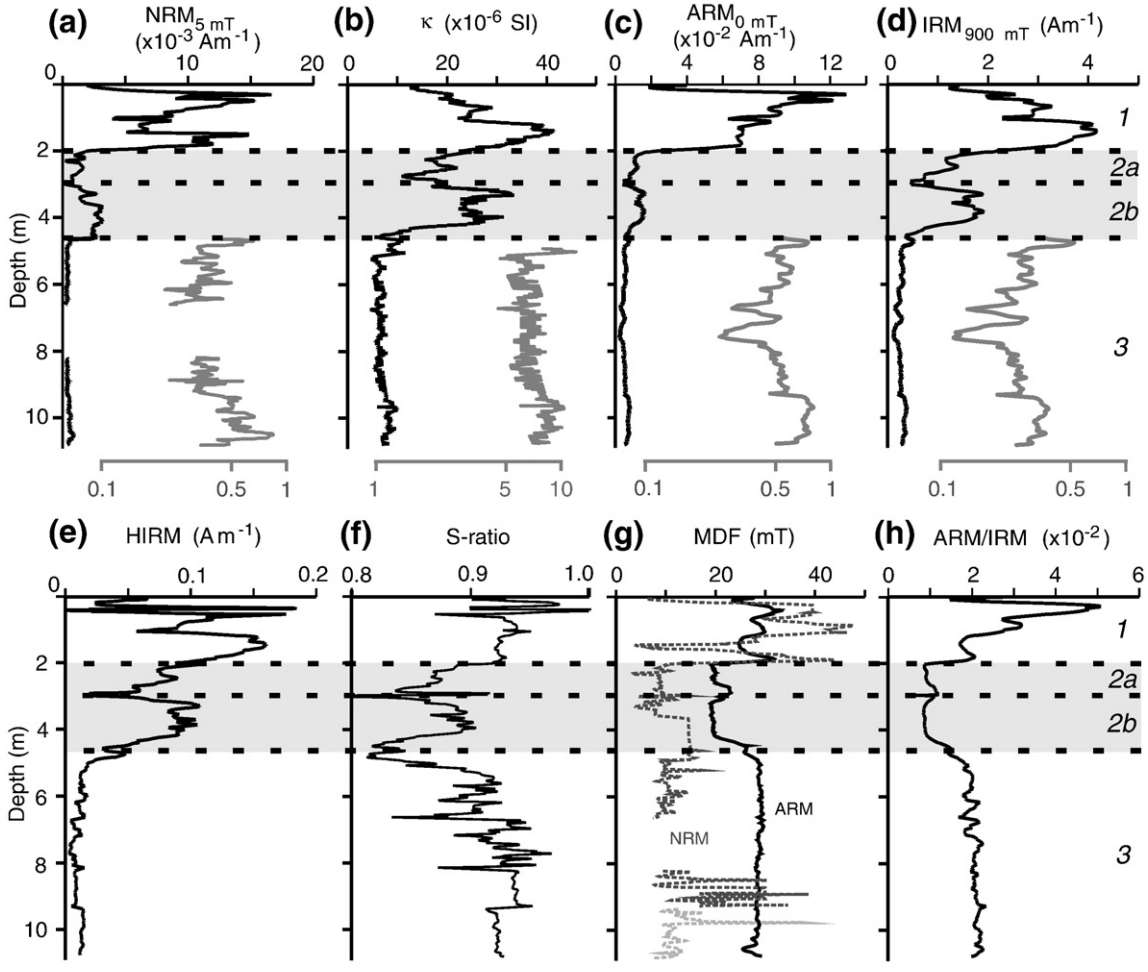

Fig. 2. Down-core variation of magnetic parameters for core CD143-55705 from the Oman margin. (a) $NRM_{5\ mT}$ (NRM is plotted following the first demagnetization step due to multiple unrecoverable flux jumps during the initial NRM measurement run; data from 6.57–8.06 m are unavailable). (b) κ, (c) ARM, (d) IRM, (e) HIRM, (f) *S*-ratio, (g) MDF_{NRM} (lighter shading indicates where calculation of MDF was complicated by magnetometer flux jumps), MDF_{ARM}, and (h) ARM/IRM. The core can be divided into three distinct zones based on systematic variations in these parameters (see Section 3.1). For (a)–(d), grey lines represent values for Zone 3 plotted on a logarithmic scale, to highlight small increases in these parameters toward the bottom of the core.

3. Results

3.1. Oman margin core CD143-55705

Abrupt down-core changes in both magnetic mineral concentration and magnetic mineralogy (Figs. 2–5) enable subdivision of the studied Oman margin core into three distinct zones, as described below.

3.1.1. Zone 1 (0–2 m)

In the uppermost 2 m of the core, concentration-dependent magnetic parameters (NRM, κ, ARM, IRM, HIRM) have high but variable average values (Fig. 2a–e). A high average *S*-ratio of 0.93 (Fig. 2f) and median destructive fields (MDFs) of ~30 mT for the NRM (Fig. 2g) suggest that the magnetic fraction in this interval is dominated by (titano-)magnetite, although HIRM values (Fig. 2e) indicate that detectable concentrations of high coercivity minerals such as hematite are also present. Declining ARM/IRM values are consistent with a coarsening in average grain size with depth, but hysteresis parameters uniformly plot toward the coarse end of the 'pseudo-single domain' (PSD) field for magnetite, on a Day plot (Day et al., 1977) (Fig. 3a). FORC distributions (Fig. 4) have a peak at B_c = 10–20 mT, and are elongated to high coercivities; the distributions also have divergent outer contours at low coercivites, indicating a mixture of non-interacting single domain (SD) and PSD (titano-)magnetite grains (Roberts et al., 2000).

In SEM images of polished sections from depths of 0.1 and 1.0 m (Fig. 5a–e), detrital titanomagnetite is the most commonly identified magnetic mineral (Fig. 5b, e). However, even at these shallow depths, minor amounts of authigenic iron sulfides are also observed. Isolated framboids are most commonly associated with the confined micro-environments inside foraminifer shells (Fig. 5a, c, d), although small aggregations are also occasionally present within the bulk sediment matrix (Fig. 5c). Whilst EDS analyses of these iron sulfides usually

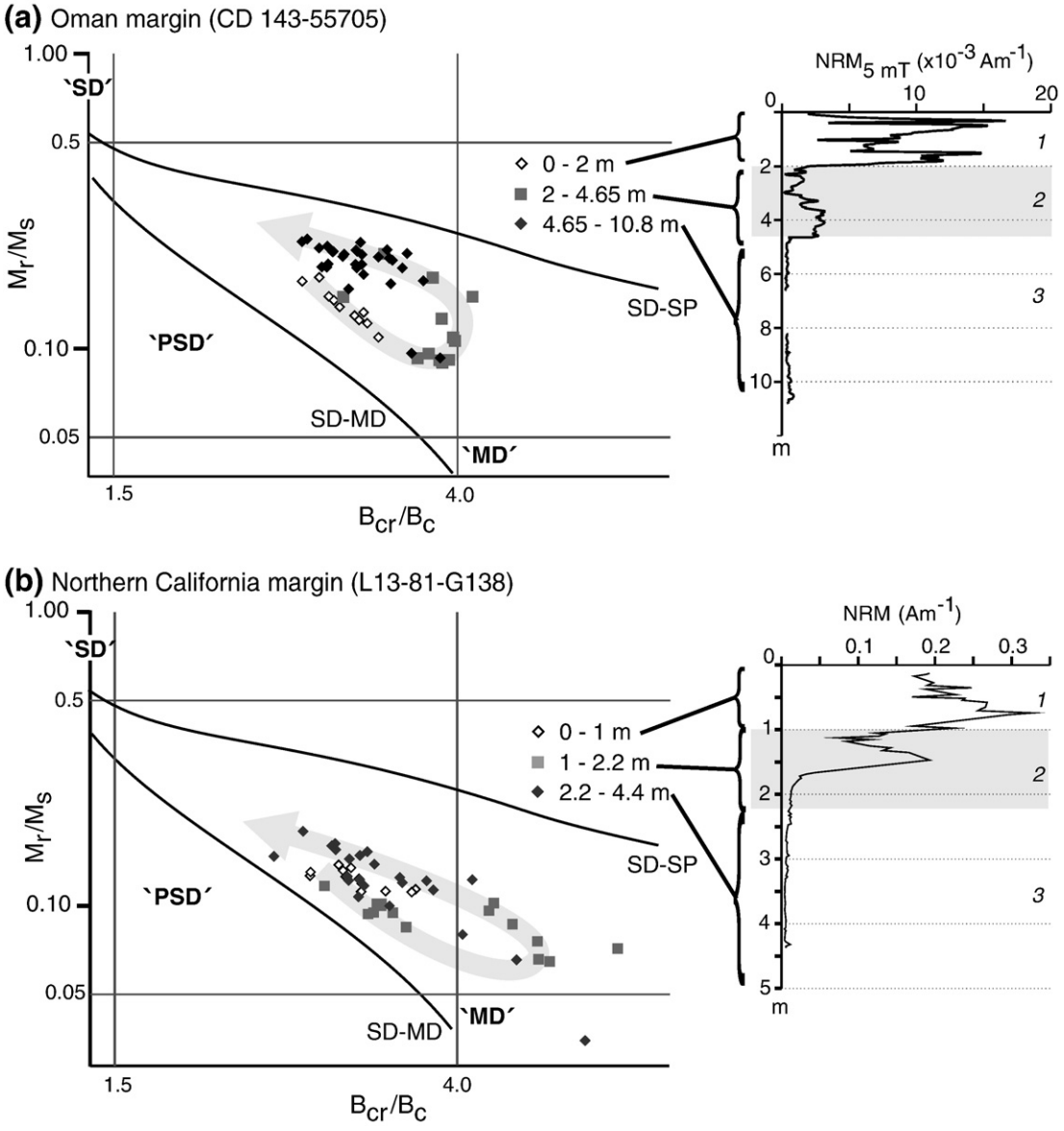

Fig. 3. Day plot (after Day et al., 1977) of hysteresis ratios for: (a) Oman margin core CD143-55705, and (b) northern California margin core L13-81-G138, illustrating the shift to higher B_{cr}/B_c values in Zone 2 (shaded grey in the accompanying plots of down-core NRM), followed by a return to more SD-like values in the lowest interval of the core (Zone 3). The association of these changes with progressive pyritization (and SEM evidence for greigite formation, as shown in Fig. 5) suggests that the observed looping is due to the progressive formation of SP greigite in Zone 2, which then grows through the stable SD blocking volume in Zone 3 (see Section 4). The theoretical SD–MD mixing curve for (titano-)magnetite is from Dunlop (2002), and the SD–SP mixing trend represents the uppermost boundary of the envelope of SD–SP mixtures from greigite-bearing sediments in New Zealand (Rowan and Roberts, 2006). The SD, PSD and MD fields for (titano-)magnetite are plotted for reference only.

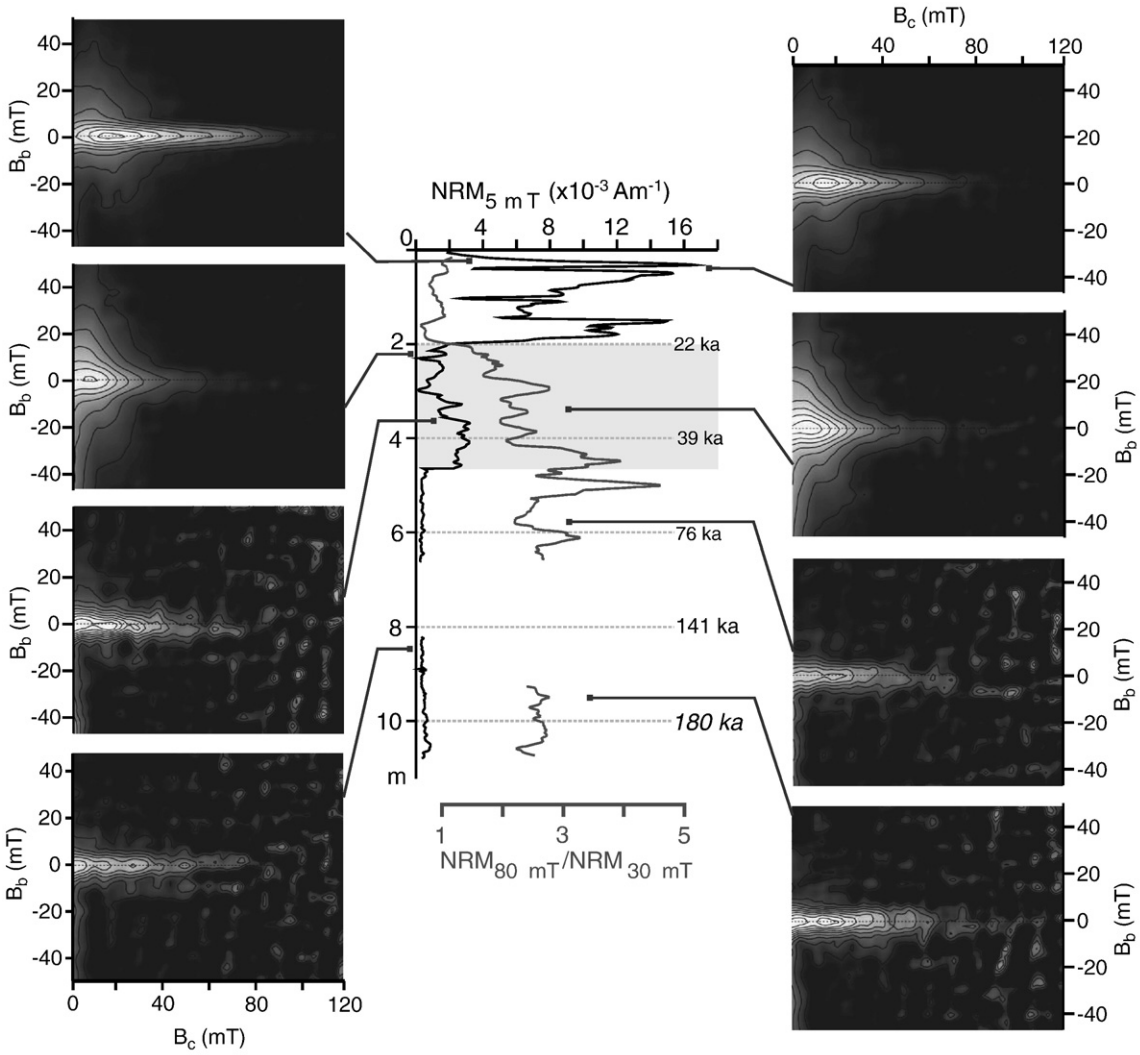

Fig. 4. Down-core changes in FORC distributions for the Oman margin core, with sample depths indicated on a plot of $NRM_{5\ mT}$. The loss and reappearance of a stable SD component in FORC distributions within Zone 2 (grey shaded region) indicates the dissolution of detrital SD magnetite followed by authigenic growth of new stable magnetic particles deeper in the sediment column; the presence of greigite is indicated by increasingly strong GRM acquisition during AF demagnetization, expressed as $NRM_{80\ mT}/NRM_{30\ mT}$ (grey line on the NRM plot; smoothed 20-point running average), and by SEM observations (Fig. 5). Sediment ages are based on correlation of foraminiferal $\delta^{18}O$ to the marine oxygen isotope record (Bryson, 2006); age control is less precise below 8 m.

indicate pyrite, a small number of smaller, finer grained framboids have greigite-like Fe:S ratios (e.g., Fig. 5c).

3.1.2. Zone 2 (2–4.65 m)

Immediately below a depth of 2 m, there is a sharp decline in concentration-dependent magnetic parameters. Parameters that are more sensitive to the presence of finer SD grains (NRM, ARM) fall by more than 80% over a 20-cm stratigraphic interval (Fig. 2a, c); parameters that are more sensitive to coarser multi-domain (MD) and PSD grains (κ, IRM) decrease more slowly (Fig. 2b, d), but also decline to a pronounced minimum at ~3 m depth. Abrupt decreases in MDF and ARM/IRM at 2 m (Fig. 2g, h) indicate the loss of magnetically stable particles at this depth. A more gradual decrease in HIRM (Fig. 2e) indicates that high coercivity minerals become less abundant, but also that they are more resistant to dissolution than magnetite. There is also a noticeable shift to higher B_{cr}/B_c values on a Day plot (Fig. 3a), and FORC distributions start to lose the peak and high B_c distribution observed in Zone 1 (Fig. 4), leaving a low coercivity distribution with divergent contours that is consistent with a dominantly PSD/MD magnetic assemblage.

Between 3 and 4.5 m, concentration-dependent magnetic parameters record a secondary peak (Zone 2b, Fig. 2). This peak is relatively minor in the NRM and ARM profiles (26% and 16% of their average values in Zone 1, respectively), and is removed entirely following demagnetization at 15 mT. The peak is much more prominent in the κ, IRM and HIRM profiles (78%, 43% and 76% of their average values in Zone 1, respectively). HIRM, *S*-ratio and MDF_{NRM} also increase in Zone 2b (Fig. 2e–g), but MDF_{ARM} and ARM/IRM remain unchanged in comparison to Zone 2a, apart from a possible small peak at ~3 m (Fig. 2g, h). These variations indicate that, compared to the uppermost part of the core, this magnetically enriched interval is proportionally richer in coarser PSD and MD grains, and high coercivity minerals such as hematite.

There is no obvious systematic difference in hysteresis parameters between Zones 2a and 2b (Fig. 3a), although two samples from depths of 3.6 to 3.8 m have significantly increased M_r/M_s and decreased B_{cr}/B_c values compared to other samples from this interval, which possibly indicates a transient change in magnetic mineralogy at the top of Zone 2b. In contrast, FORC distributions indicate a permanent alteration of the magnetic mineral assemblage below depths of approximately 3.5 m (Fig. 4): the coercivity distribution clearly extends to much higher values, but is now narrowly confined around the B_b axis even at

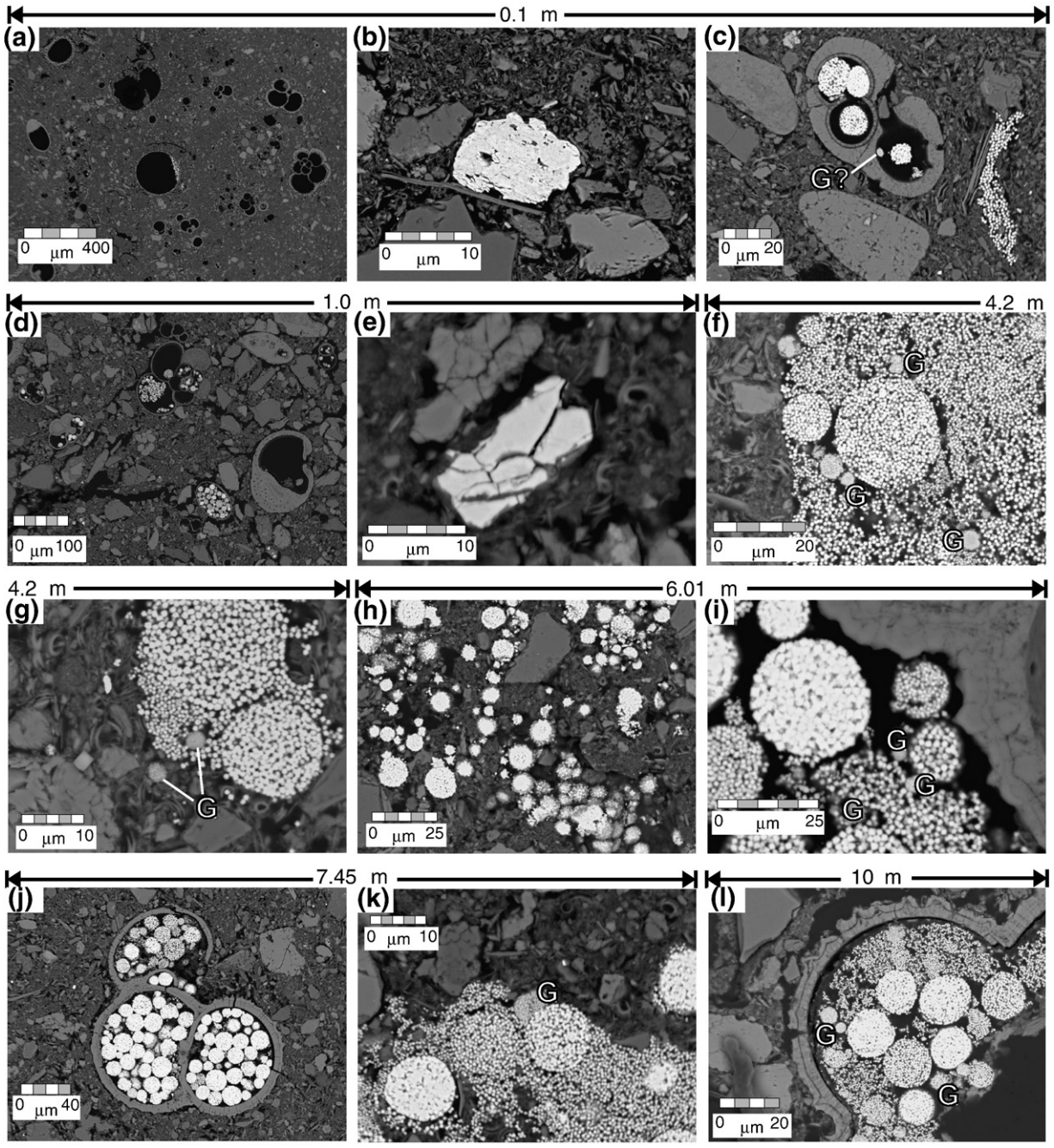

Fig. 5. Backscattered electron micrographs from 6 selected intervals in the Oman margin core ((a)–(e) Zone 1; (f), (g) Zone 2; (h)–(l) Zone 3). (a) Wide-field view illustrating the general absence of authigenic iron sulfides at 0.1 m. (b) Detrital titanomagnetite grain at 0.1 m. (c) Individual pyrite and possible greigite (G) framboids inside a microfossil at 0.1 m, and non-framboidal pyrite within the sediment matrix. (d) Wide-field view indicating iron sulfides starting to fill microfossils at 1.0 m. (e) Detrital magnetite grain with corroded edges at 1.0 m. (f) Large iron sulfide aggregate with an early generation of pyrite framboids and a later, space-filling generation, including small greigite framboids at 4.2 m. (g) Close-up of a smaller iron sulfide aggregate, with similar growth patterns to (f), at 4.2 m. (h) Wide-field view illustrating high concentrations of pyrite framboids, commonly with euhedral overgrowths, within the sediment matrix at 6.01 m. (i) Close-up of an early pyrite framboid with euhedral overgrowths, surrounded by later space-filling pyrite and greigite at 6.01 m. (j) Microfossil filled with euhedrally overgrown pyrite framboids at 7.45 m. (k) Close-up of an iron sulfide aggregate within the sediment matrix, with a large patch of gregite neoforming around a pyrite framboid at 7.45 m. (l) Close-up of an iron sulfide aggregate within a microfossil at 10 m, with later space-filling pyrite and greigite surrounding euhedrally overgrown pyrite framboids.

low coercivities. SEM observations from a depth of 4.2 m in Zone 2b (Fig. 5f, g) clearly indicate the growth of large concentrations of iron sulfides as aggregates within the sediment matrix. Most of these aggregates are the product of at least two generations of iron sulfide growth, with a space filling phase surrounding an earlier generation of framboids. Greigite, identified on the basis of markedly higher Fe:S ratios on EDS spectra (compared to that expected for pyrite), principally occurs in fine-grained patches associated with this later phase of growth.

3.1.3. Zone 3 (4.65–10.8 m)

The lowermost part of the Oman margin core is characterized by a highly attenuated magnetic signal, with the values of all concentration-dependent magnetic parameters below a depth of ~4.5 m reduced to 12% or less of the average values observed in Zone 1 (Fig. 2a–e). When plotted on a logarithmic scale (grey lines, Fig. 2a–d) small variations are still apparent, and a small but gradual increase in NRM and ARM intensities is indicated below ~9.2 m. This increase is less obvious in the IRM and κ profiles, which suggests that the

increases in NRM and ARM represent an enhancement of magnetic grains in the SD size range toward the base of the core.

Other changes at the top of Zone 3 include sharp increases in *S*-ratio, MDF_{ARM} and ARM/IRM (Fig. 2f–h), and a systematic shift in hysteresis parameters to B_{cr}/B_c values comparable with, and M_r/M_s values slightly higher than, those observed in Zone 1 (Fig. 3a). These changes are consistent with an increased proportion of thermally stable SD magnetic grains within Zone 3. *S*-ratio and ARM/IRM continue to gradually increase with depth, whereas hysteresis ratios and MDF_{ARM} remain constant. MDF_{NRM} exhibits considerable variability, with values initially lower than those in Zone 2b but apparently increasing below 9 m (values in the lower part of Zone 3 were difficult to estimate due to unrecoverable magnetometer flux jumps during measurement). FORC distributions remain unchanged from the pattern first observed at the bottom of Zone 2 (Fig. 4). SEM observations indicate that aggregates of authigenic iron sulfides become larger and more abundant with depth (Fig. 5h–l). These aggregates are still composed of distinct early framboidal and later space-filling generations of iron sulfides; any greigite present is associated with the later episodes of growth. Euhedral overgrowth of the early pyrite framboids is also commonly observed (e.g., Fig. 5k). Together, these observations suggest that authigenic growth of iron sulfides is occurring throughout Zone 3.

3.2. Northern California margin core L13-81-G138

Although data for the studied northern California margin core (Figs. 3b, 6 and 7) are less comprehensive and have lower resolution than those for the Oman margin core, particularly below depths of 1.5 m, down-core variations in magnetic parameters exhibit similar patterns to those discussed above, with an upper interval that has high magnetic mineral concentrations (Zone 1, Fig. 6: 0–1 m) overlying a transition zone (Zone 2: 1–2.2 m) to an interval with low magnetic mineral concentrations in the lowermost part of the core (Zone 3: 2.2–4.4 m). Magnetic parameters that are sensitive to SD grains (NRM, ARM) decrease sharply within two specific intervals, at 0.8–1.1 m and 1.5–1.7 m (Fig. 6a, c); there is a secondary peak in NRM intensities at 1.5 m (low data resolution makes it impossible to tell if there is a matching ARM peak). In contrast, parameters that are more sensitive to the presence of PSD/MD grains (κ, IRM_{900}) only undergo a single noticeable decrease between 1.5 and 2 m, over a slightly broader depth interval than the associated NRM decrease. There is a local minimum in IRM_{900} intensity at ~1 m depth (Fig. 6d), but κ increases throughout the upper third of the core down to 1.5 m (Fig. 6b). When concentration-dependent parameters are plotted on a logarithmic scale for Zone 3 (grey lines, Fig. 6a–d), there appear to be slight increases in NRM, ARM and IRM_{900} just above the base of the core; ARM/SIRM also slightly increases below 3 m (Fig. 6f).

Other magnetic parameters also vary in a manner comparable to that observed in the Oman margin core. MDF values (Fig. 6e) are high (40–50 mT) but gradually decrease with depth in Zone 1. MDF_{NRM} drops by 50% between 1 and 1.2 m, then after a minor secondary peak at 1.3 m continues to slowly decrease, before levelling out at 10 mT below 3 m. MDF_{ARM} reaches a minimum at 1.5 m, then increases to higher values (~40 mT) in the bottom 2 m of the core. On a Day plot

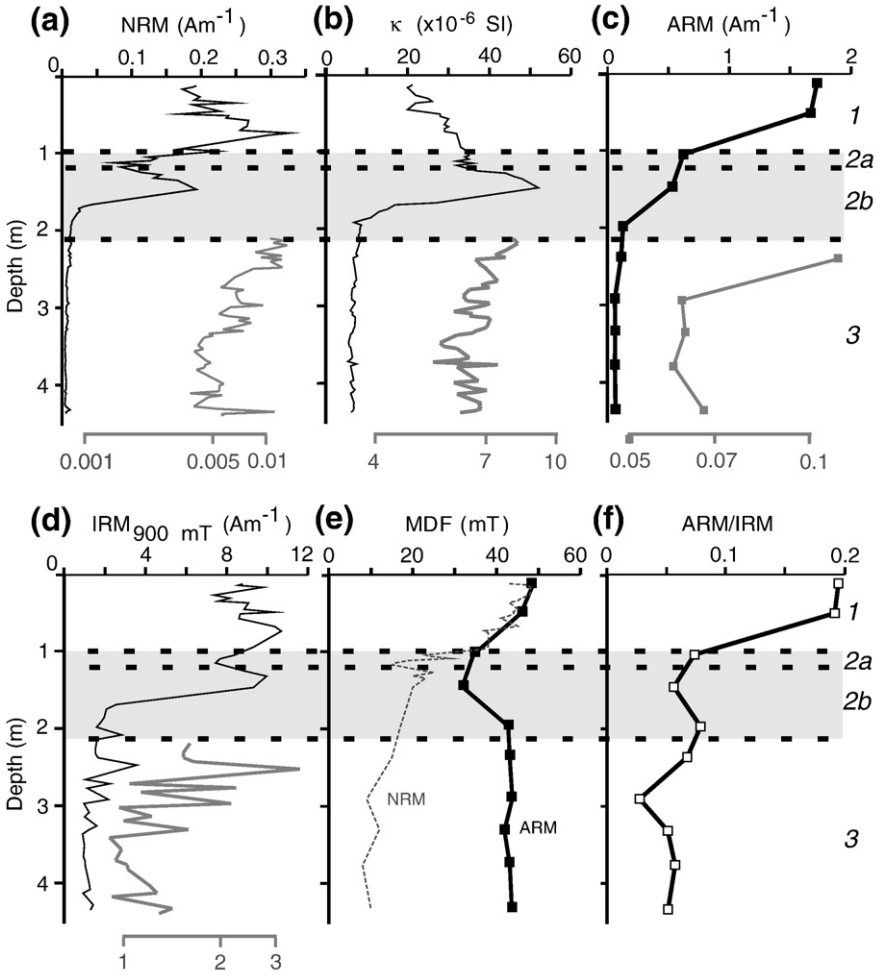

Fig. 6. Down-core variation of magnetic parameters for core L13-81-G138 from the northern California margin. (a) NRM, (b) κ, (c) ARM, (d) IRM, (e) MDF_{NRM}, MDF_{ARM}, and (f) ARM/IRM. Similar changes to those observed in the Oman margin core allow a similar division into three zones. The grey lines in (a)–(d) represent values for Zone 3 on a logarithmic scale.

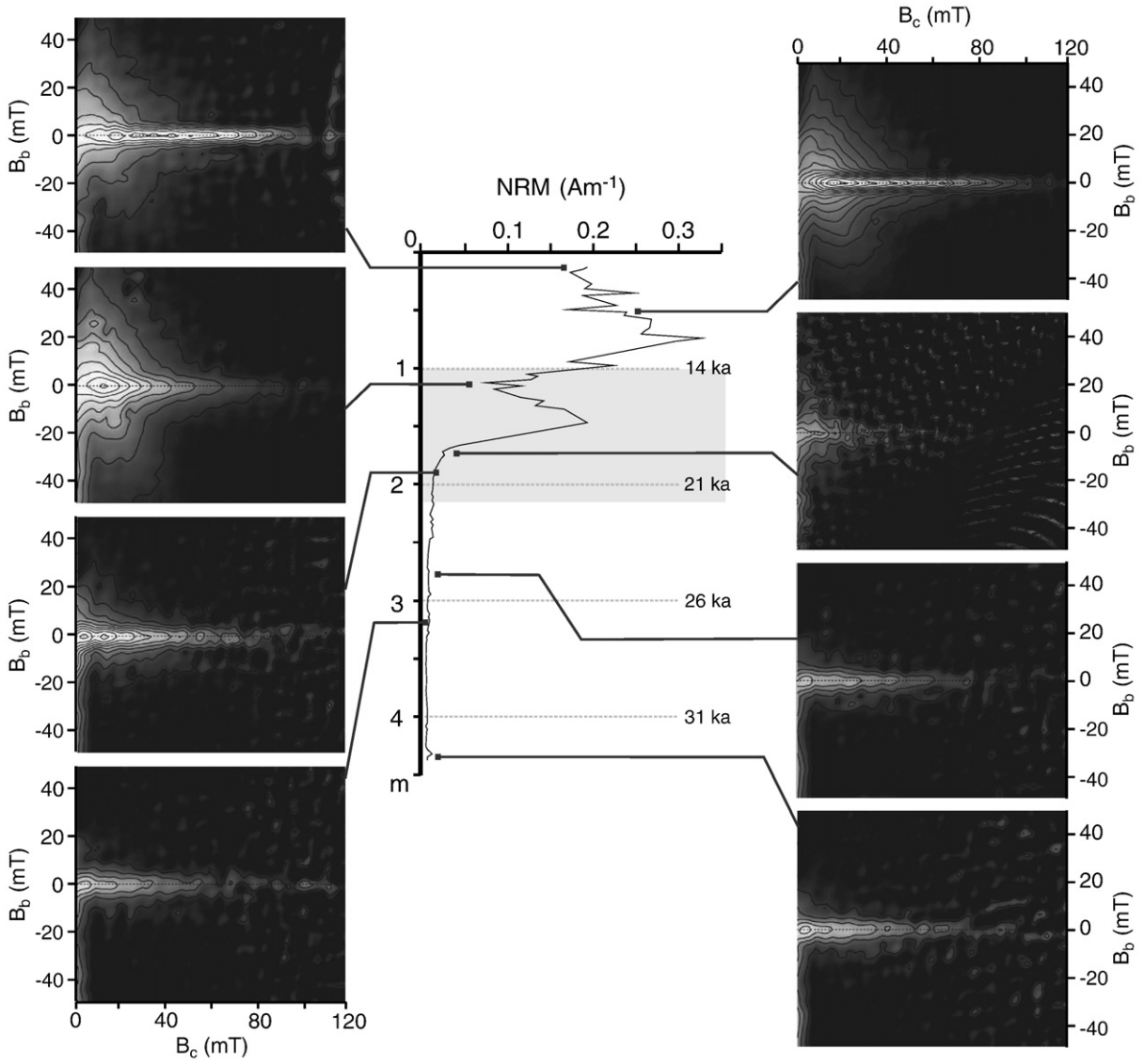

Fig. 7. Down-core changes in FORC distributions for the studied northern California margin core, illustrating the same loss and reappearance of a stable SD component within Zone 2 (grey shaded region) as is observed for the Oman margin core (Fig. 4). Sediment ages are extrapolated from the AMS ^{14}C ages of Gardner et al. (1997).

(Fig. 3b) hysteresis parameters exhibit down-core looping behavior, with coarse PSD magnetite-like values within Zone 1, a transition to much higher B_{cr}/B_c values within Zone 2, and a transition back to lower B_{cr}/B_c, and slightly higher M_r/M_s values, in Zone 3. FORC distributions for the upper part of the core (Fig. 7) indicate a magnetic assemblage composed of a high coercivity non-interacting SD component and a low coercivity PSD/MD component, with a peak at ~20 mT. The high coercivity distribution disappears between 1 and 1.7 m, along with the PSD/MD component. Below ~1.9 m, the FORC distributions indicate the appearance of a magnetically non-interacting higher coercivity component; the distribution is centered on the origin of the FORC diagram, which indicates that there is also a substantial superparamagnetic (SP) contribution (Pike et al., 2001).

4. Discussion

4.1. Interpretation of diagenetic trends

Anaerobic degradation of organic matter in marginal and pelagic sedimentary environments is known to cause dissolution of detrital magnetic minerals and authigenic growth of iron sulfides (Karlin and Levi, 1983, 1985; Canfield and Berner, 1987; Karlin, 1990a,b; Leslie et al., 1990a,b; Channell and Hawthorne, 1990; Bloemendal et al., 1992; Tarduno, 1992; Bloemendal et al., 1993; Roberts and Turner, 1993; Tarduno, 1994; Dekkers et al., 1994; Robinson et al., 2000; Larrasoaña et al., 2003; Liu et al., 2004; Emiroglu et al., 2004; Rey et al., 2005; Rowan and Roberts, 2006). Variations in magnetic properties consistent with the progressive down-core dissolution of detrital Fe–Ti oxide mineral grains and associated authigenic formation of iron sulfide minerals are observed in both of the studied sediment cores. These cores lack pore water chemistry data, but combining the rock magnetic data with SEM observations from the Oman margin (Fig. 5) helps to establish a basic diagenetic zonation (Fig. 8a), because the observed authigenic minerals can be clearly linked to the geochemistry of the sedimentary environment (Berner, 1981).

The primary magnetic mineral assemblage in Zone 1, which is dominated by detrital SD and PSD (titano-)magnetite, undergoes almost complete dissolution in Zone 2 (Figs. 2 and 6). The early occurrence of minor amounts of pyrite within the sediment matrix of the Oman margin core (Fig. 5c) indicates that anoxic conditions were established close to the sediment–water interface (cf. Berner, 1981), and that the oxic and suboxic zones must be very thin. However, the persistence of detrital titanomagnetite grains, albeit with corroded rims (Fig. 5e), and the low overall abundance of iron sulfides in the

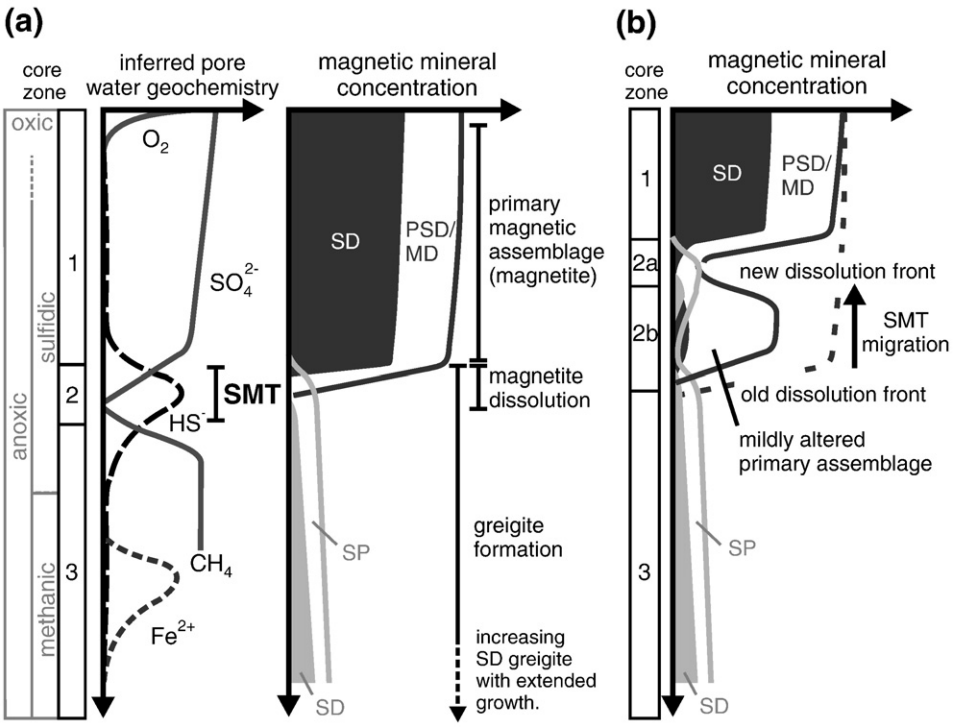

Fig. 8. (a) Simplified model of inferred down-core changes in magnetic mineral content of the studied cores, illustrating the progressive dissolution of SD and PSD magnetite (dark grey area/line) and formation of SP/SD greigite (light grey line/area) at the sulfate–methane transition (SMT); the delay before greigite grows to SD size; and continuous greigite growth in Zone 3. High coercivity minerals (e.g., hematite) have been excluded for the sake of clarity, but would be expected to follow the progressive down-core dissolution trend described by (Liu et al., 2004). (b) Model incorporating a recent upward migration of the SMT in the sediment column, leaving an interval enriched in PSD/MD magnetite (Zone 2b) between the old and new dissolution fronts.

uppermost part of the sediment column suggest that rates of sulfate reduction remained low above Zone 2. Accelerated magnetite dissolution and concomitant formation of authigenic iron sulfides observed in Zone 2a are most likely to be associated with the sulfate–methane transition (SMT; Fig. 8a), where upward diffusion of biogenic (and possibly thermogenic) methane from deeper in the sediment column provide an additional source of organic carbon for sulfate-reducing bacteria, producing a peak in pore water H_2S concentrations (Kasten et al., 1998; Neretin et al., 2004; Jørgensen et al., 2004).

Toward the base of Zone 2, increased MDF_{ARM} and ARM/IRM values (Figs. 2g, h and 6e, f), the reappearance of a high coercivity component in FORC diagrams (Figs. 4 and 7), and the looping back to more SD-like values on a Day plot (Fig. 3) all indicate formation of new magnetically stable grains at depth. SEM observations indicate that the most likely explanation for this magnetic enhancement is the growth of magnetically stable greigite, which is observed in increasing quantities at these depths (Section 3.1.3). The offset between this transition, and the zone of most intense reductive diagenesis at the top of Zone 2, can be explained by the fact that newly formed greigite particles will initially be small and exhibit thermally unstable SP behavior; it will take some time before easily detectable quantities grow through the stable SD blocking volume. Nucleation of SP greigite in the upper part of Zone 2 could cause the observed shift to higher B_{cr}/B_c values (Dunlop, 2002), an effect that has been previously documented in greigite-bearing sediments from New Zealand (Rowan and Roberts, 2006) (Fig. 3). The looping of hysteresis parameters observed in Zone 2 may therefore be largely due to the effects of authigenic greigite growth, rather than being the sole result of changes in the detrital magnetic assemblage (although both processes are occurring). A further indication of greigite formation at the top of Zone 2 in the Oman margin core is the acquisition of a minor but increasingly large gyroremanent magnetization (GRM), indicated by a down-core increase in $NRM_{80\ mT}/NRM_{30\ mT}$ in Fig. 4, which is a characteristic of SD greigite (Snowball, 1997; Sagnotti and Winkler, 1999). This acquisition of a weak GRM indicates that small amounts of greigite have probably already grown through the SD blocking volume at the top of Zone 2, which suggests that the $NRM_{80\ mT}/NRM_{30\ mT}$ parameter is considerably more sensitive to the presence of thermally stable greigite than the other rock magnetic parameters used in this study.

Greigite formation in Zone 2 is volumetrically insignificant compared to the amount of detrital magnetite being removed by dissolution; most dissolved iron is taken up by paramagnetic pyrite, which does not record a paleomagnetic signal. Zone 3 is therefore characterized by extremely low concentrations of thermally stable magnetic grains and a weak NRM. Hysteresis ratios and FORC distributions are unchanged throughout this interval (Figs. 3, 4 and 7). However, in the Oman margin core, the *S*-ratio and ARM/IRM continue to increase with depth (Fig. 2f, h), which indicates ongoing enrichment in SD grains toward the bottom of the core. Widespread euhedral overgrowth of early pyrite framboids (Fig. 5k) indicates continued iron sulfide growth in evolving pore waters (Raiswell, 1982), and increases in concentration-dependent magnetic parameters toward the bottom of both cores (Figs. 2a–d and 6a–d) also indicates continuous, but slow, growth of greigite through the stable SD blocking volume throughout Zone 3 (Fig. 8a). This matches similar observations for sediment cores from the Korea Strait (Liu et al., 2004). The precise mechanism of iron sulfide growth so far below the SMT, where exhaustion of the sulfate supply should inhibit pyritization, is unclear. Limited amounts of sulfide must be present in the pore water, possibly by downward diffusion, or as a product of anaerobic pyrite oxidation (Bottrell et al., 2000; Larrasoaña et al., 2007). Importantly, such sulfide limitation would favor the early arrest of pyritization, and preservation of greigite (Kao et al., 2004).

4.2. SP enhancement during reductive diagenesis

Given that progressive dissolution of detrital magnetic iron oxide minerals is accepted as a fundamentally important process in reducing

environments, it was surprising when Tarduno (1995) found enhanced concentrations of ultra-fine grains exhibiting SP behavior in diagenetically reduced sediments. Our analysis confirms that SP enhancement can occur in anoxic diagenetic settings, and suggests that it is due to the formation of authigenic greigite. Growth of greigite from solution will proceed from an initial extremely fine-grained nucleus through to a size that is large enough to exceed the stable SD blocking volume (cf. Rowan and Roberts, 2006). In the sulfate-limited diagenetic environment below the SMT, it would not be surprising for greigite growth to be arrested and for fine-grained greigite to exhibit dominantly SP behavior. Rowan and Roberts (2006) reported that SP greigite is abundant in the spatially extensive and thick Neogene stratigraphic successions of reduced marine sediments exposed throughout eastern New Zealand. We suggest that authigenic greigite growth, as has been inferred within Zones 2 and 3 of the studied Oman and California margin cores, is also responsible for the diagenetic SP enhancement documented by Tarduno (1995).

4.3. Evidence for SMT migration within the sediment column

Magnetic profiles for both studied cores contain two distinct decreases in magnetization within Zone 2, at ~1.8–2 m and ~4–4.6 m in the Oman margin core, and at ~0.8–1 m and ~1.5–2 m in the northern California margin core, which we interpret as two separate dissolution fronts. This is not a feature of the idealized model of coupled magnetite dissolution and iron sulfide formation presented in Fig. 8a. The interval between the inferred dissolution fronts (Zone 2b) is relatively enriched in PSD/MD magnetite and high-coercivity magnetic minerals, suggesting that fine SD grains have been preferentially removed by dissolution. Coarser magnetite grains with a lower surface area to volume ratio will react more slowly with dissolved sulfide, and hematite has been shown to persist longer than magnetite in sulfidic environments (e.g., Yamazaki et al., 2003; Emiroglu et al., 2004; Liu et al., 2004; Garming et al., 2005; Rey et al., 2005). However, although the lower inferred reactivity of hematite and coarser detrital magnetite grains can account for the slower decay of κ, IRM and HIRM with depth observed within both dissolution fronts, they cannot explain the secondary peak in magnetic mineral concentration in Zone 2b, which indicates that this interval has been subjected to less intense reductive diagenesis than the overlying Zone 2a. A similar magnetic signature has been documented in sediments from the Argentine margin, where the SMT has migrated upward in the sediment column in response to an order-of-magnitude decrease in sedimentation rate at the beginning of the Holocene (Riedinger et al., 2005). Garming et al. (2005) reported that the modern SMT on the Argentine margin is located at a pronounced minimum in concentration-dependent magnetic parameters, beneath which is an interval that was initially above the zone of reductive diagenesis, and has been mildly altered during, and since, the ascent of the SMT to its present position. The minimum in magnetic mineral concentration observed within Zone 2a of the Oman and northern California margin cores may therefore mark the current position of the SMT following a recent ascent from the lower dissolution front at the top of Zone 3 (Fig. 8b). This migration was most probably a response to environmental changes at the beginning of the Holocene; sedimentation rates in both cores have decreased since the last glacial maximum, and changes in other environmental factors such as marine C_{org} productivity may also have altered the geochemical/pore water equilibrium within the sediment column. Dissolution of the originally pristine magnetic assemblage in Zone 2b is occurring at a slower rate than in Zone 2a due to lower H_2S concentrations; sufficient time has elapsed since SMT migration to almost completely dissolve fine-grained SD magnetite in this interval, but coarser-grained magnetite and hematite have yet to fully dissolve.

4.4. Timescales of magnetic iron sulfide growth

Chronologies established for both the Oman and northern California margin cores, using foraminiferal $\delta^{18}O$ (Bryson, 2006) (Fig. 4) and AMS ^{14}C dating (Gardner et al., 1997) (Fig. 7), respectively, provide constraints on the timing of the observed down-core diagenetic changes (Table 1). A pristine detrital magnetic record is only preserved in the uppermost part of these cores, above the SMT. In sediments older than 10–20 kyr, this detrital signal has been destroyed and newly-formed authigenic greigite becomes the dominant magnetic carrier, resulting in a substantial temporal offset and smoothing of the recorded paleomagnetic signal. The delay in remanence acquisition corresponds to the age of the sediments toward the bottom of Zone 2, where the first stable SD greigite is detected. This presently occurs at 34 kyr in the Oman margin core, and at 20 kyr in the northern California margin core, indicating that the remanent magnetization in sediments below the SMT is tens of thousands of years younger than the surrounding host sediments. Mobility of the SMT within the sediment column over glacial–interglacial timescales will cause this age offset to vary over time. The population of magnetically stable greigite particles gradually increases with depth in Zone 3, as more greigite grows through the SD blocking volume. The magnetization of later-forming greigite will have an even larger age offset with respect to the host sediment, and the total remanent magnetization of a particular volume of sediment will be the vector sum of remanences acquired over the entire interval of

Table 1
Estimated timescales of authigenic greigite growth for cores shown in Fig. 1

Core (location, water depth)	Holocene sed. rate	Magnetite dissolution/ outward loop	First SD greigite/ inward loop	Duration of SD greigite formation	Reference
	(cm/kyr)	(kyr)	(kyr)	(kyr)[a]	
Greigite directly observed/inferred					
CD143-55705 — Oman margin (22°22′N 60°08′E, 2193 m)	6–8	22	34	≥160	This study
L13-81-G138 — N California margin (38°25′N 123°58′W, 2531 m)	6–7	14	20	≥14	This study
SSDP-102 — Korea Strait (34°57′N 128°53′E, 40 m)	230	0.3	1	≥5	(Liu et al., 2004)
SP enhancement associated with sulfate reduction					
ODP-806A — Ontong–Java Plateau (00°19′N 159°22′E, 2520 m)	2	475	525	≥25	(Tarduno, 1994, 1995)
GeoB-4901[b] — Niger Fan (02°41′N 06°43′E, 2184 m)	5–12	120	>220	unknown	(Dillon and Bleil, 2006)
Looping of hysteresis parameters only					
W7905A-121 — Oregon (45°15′N 125°00′W, 919 m)	120	0.25	0.6	≥1	(Karlin, 1990a)
GH 98-1232 — Japan Sea (44°48′N 139°42′E, 838 m)	20	6	7	≥1	(Yamazaki et al., 2003)
GeoB-6229[c] — Argentine margin (37°12′S 52°39′W, 3446 m)	3–7	13	13.5	~3	(Garming et al., 2005)

[a] Age estimates assume that the looping of hysteresis parameters in the published records is diagnostic of greigite formation, illustrating the large but extremely variable resulting offset and smoothing of the paleomagnetic signal.
[b] Core does not extend to base of sulfidic anoxic zone.
[c] Core does not extend to position of dissolution front prior to SMT migration.

greigite growth. The minimum estimated duration for this smoothing interval is ~15 kyr for the northern California margin core, and ~160 kyr for the Oman margin core. However, we cannot rule out continued greigite formation below the cored intervals in these locations, which would result in even greater paleomagnetic smoothing deeper in the sediment column.

4.5. Similar down-core patterns in globally distributed records

Greigite formation during early diagenesis has not been widely documented in previous studies of active depositional systems, even though magnetite dissolution coupled with sulfate reduction and pyrite formation are well-known phenomena. Exceptions include Liu et al. (2004), who detected greigite in the lowermost interval of cores from the Korea Strait, and interpreted gradual down-core increases in NRM and *S*-ratio throughout the lower part of core SSDP-102 as indicating greigite growth over an extended interval in the sediment column. Although not discussed by Liu et al. (2004), their hysteresis data follow a looping trajectory on a Day plot through the interval in which detrital magnetite is being replaced by greigite (Fig. 9). Diagenetic trends documented in the Korea Strait are therefore directly comparable to those observed on the Oman and northern California margins. The global distribution of these three records (Fig. 1) indicates that geochemical conditions that favor the formation and preservation of greigite can be achieved relatively easily during early diagenesis.

Furthermore, hysteresis parameters from other published records (Figs. 1 and 9) indicate that down-core looping of hysteresis parameters on a Day plot, associated with sulfate reduction, is routinely observed in anoxic diagenetic settings. Such data have commonly been interpreted solely in terms of changes in the detrital magnetite assemblage: the outward loop toward higher B_{cr}/B_c values is generally interpreted to represent an increasing proportion of coarse PSD and MD magnetite as finer SD magnetite is preferentially dissolved, while the return loop has been interpreted to represent the fining and fragmentation of these coarser particles with prolonged exposure to H_2S (e.g., Karlin, 1990a; Yamazaki et al., 2003; Garming et al., 2005). However, close association of these changes with growth of authigenic pyrite in these cores raises the possibility that, as has been inferred for the records described in this paper, the outward loop toward higher B_{cr}/B_c values, which would normally be considered to indicate "coarser" grain sizes, is caused by the nucleation of fine SP greigite during sulfate reduction, in addition to dissolution of SD detrital magnetite. The return loop would then mark the progressive growth of greigite through its SD blocking volume to produce a mixture of SD and SP greigite. In the records examined, the trajectories of the loops on a Day plot typically have a noticeably shallower gradient than theoretical SD–MD mixing trends for magnetite (Dunlop, 2002), and the return portions of most loops fall within the SP–SD mixing envelope for greigite-bearing sediments reported by Rowan and Roberts (2006) (Figs. 3 and 9). SP enhancement has been directly detected in the interval characterized by higher B_{cr}/B_c values (the outward part of the loop), and increased pore water H_2S concentrations, in sediments from the Ontong–Java Plateau (e.g., Tarduno, 1994, 1995; it should be noted that pore water geochemistry for this core is based on correlation to adjacent holes rather than direct measurements) and the Niger Fan (Dillon and Bleil, 2006) (Fig. 9). In both of these cores, magnetite dissolution at the iron-redox boundary higher in the sediment column produced no significant change in hysteresis ratios, which further suggests that the looping observed in the sulfate reduction zone may be linked to greigite formation rather than to dissolution of the primary magnetic assemblage. In both cases, the mineral causing the SP enhancement is unknown, although Dillon and Bleil (2006) acknowledged that greigite is possibly present in the Niger Fan sediments. Therefore, for many of these records, the looping of hysteresis parameters may indicate progressive growth of small, but paleomagnetically significant, quantities of greigite during sulfate reduction. Potential timescales of greigite growth can be estimated by assuming that the return loop marks the first appearance of SD greigite. This indicates a wide range of paleomagnetic offsets and smoothing intervals (Table 1).

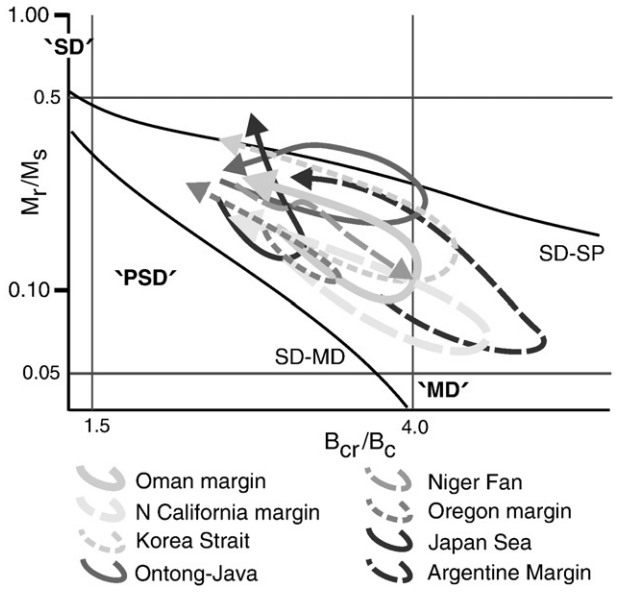

Fig. 9. Day plot (cf. Day et al., 1977) illustrating the progressive down-core looping of hysteresis parameters associated with sulfate reduction in numerous marine sediment records from anoxic environments, including the trajectories for the Oman and northern California margin cores. See Table 1 or Fig. 1 for references. SD–SP and SD–MD mixing lines are as in Fig. 3.

4.6. Are the above processes ubiquitous in reducing sediments?

The dominant iron sulfide species that forms during early sediment diagenesis will depend on the balance between key reactants, principally C_{org}, dissolved sulfide and reactive iron (e.g., Berner, 1984; Roberts and Turner, 1993; Kao et al., 2004). When C_{org} and dissolved sulfide are abundant, dissolved reactive iron will be completely sulfidized and pyrite will be the dominant authigenic sulfide formed. This appears to be the case in the studied cores (Fig. 5); nevertheless, greigite is also present in small quantities, possibly due to eventual exhaustion of sulfide during pyritization. The small amount of SP/SD greigite formed only results in a small, superposed magnetic enhancement. However, because most of the detrital ferrimagnetic mineral assemblage has been replaced by paramagnetic pyrite, this weak authigenic magnetization can still be paleomagnetically significant (e.g., Rowan and Roberts, 2006, 2008). The global distribution of records (Fig. 1) where looping of hysteresis parameters is observed (Fig. 9) suggests that the observed growth of SP/SD greigite during progressive magnetite dissolution may be widespread.

At the other end of the spectrum, most previous reports of sedimentary greigite are from environments in which the growth of dominantly SD greigite has given rise to strong magnetizations (e.g., Tric et al., 1991; Horng et al., 1992; Roberts and Turner, 1993; Florindo and Sagnotti, 1995; Snowball, 1997; Horng et al., 1998; Sagnotti and Winkler, 1999; Jiang et al., 2001; Roberts et al., 2005; Sagnotti et al., 2005; Larrasoaña et al., 2007; Vasiliev et al., 2007). In such environments, it is likely that reactive iron was abundant and sulfide was limited (Kao et al., 2004), preventing sulfidization reactions from going to completion. The early arrest of pyrite formation will lead to more greigite being preserved, and stronger magnetizations. It is therefore the interplay between concentrations of the key reactants that will dictate the concentration magnetic characteristics of authigenic greigite. Regardless, our observations indicate that late

growth of greigite after destruction of the detrital magnetic mineral assemblage will be common in organic-rich marginal and pelagic settings. The magnetic characteristics of SP-dominated greigite mixtures, such as in the cores studied here, are much less distinctive than those of sediments dominated by SD greigite, making it likely that their presence has been under-recognized in the geological record. For example, Yamazaki et al. (2003) argued against greigite formation in reduced sediments from the Japan Sea based on a lack of GRM acquisition, but acquisition of minor GRMs, similar to those observed for greigite-bearing sediments in this study, is indicated in their Fig. 4 (samples at depths of 2.51 and 3.21 m). We therefore argue that the processes documented in the present study will become more widely recognized in future.

5. Conclusions and implications for the magnetic record in anoxic marine sediments

Bacterially-mediated sulfate reduction and pyritization during early diagenesis of rapidly deposited sediments from the Oman and northern California margins has led to the complete dissolution of detrital magnetite, and its replacement by greigite as the principal magnetic mineral. Following destruction of the primary magnetic assemblage, FORC distributions and down-core increases in the *S*-ratio and MDF_{ARM} indicate the appearance of a new population of thermally stable magnetic particles, which SEM observations confirm to be greigite. Hysteresis parameters follow a looping trajectory on a Day plot (Day et al., 1977) through the transition zone, as a result of the nucleation of superparamagnetic greigite at the magnetite dissolution front and its later growth through the stable single domain blocking volume. Increases in concentration-dependent magnetic parameters toward the bottom of both cores indicate that growth of new greigite may continue deep into the sediment column, producing a remanent magnetization that is not only offset from the age of the host sediments by 10's of kyr, but which is also a smoothed record of 10's or even 100's of kyr of magnetic field behavior. The environmental magnetic and paleomagnetic signals in these cores are likely to be severely compromised by such diagenetic effects. SP-dominated mixtures may represent the most common natural occurrence of greigite, but they can be difficult to detect using discrimination methods that assume dominantly SD behavior (e.g., Roberts, 1995; Snowball, 1997; Sagnotti and Winkler, 1999); similar patterns of rock magnetic variations seen in numerous other records from similar sedimentary environments may therefore also indicate paleomagnetically significant quantities of greigite. Late remagnetizations are recognized as a common problem in greigite-bearing sediments (Roberts and Weaver, 2005; Rowan and Roberts, 2008), but our results suggest that even in ideal cases where the magnetic signal is carried entirely by early diagenetic greigite, there is likely to be a substantial offset between the age of the magnetization and the host sediment, and considerable smoothing of recorded magnetizations.

Acknowledgements

We thank Richard Pearce for invaluable assistance with SEM analysis at NOCS, Jim Gardner, formerly of the US Geological Survey, Menlo Park, California, for providing access to core L13-81-G138, and Ken Verosub for shipping the samples to NOCS for further analysis. Work on core L13-81-G138 was performed by APR when employed at the University of California, Davis, and was funded by the Western Regional Center of the National Institute for Global Environmental Change of the U.S. Department of Energy. Fig. 1 was generated using the GMT package. We thank L. Sagnotti, P. Delaney and two anonymous reviewers for helpful reviews.

Appendix A. Supplementary data

Supplementary data associated with this article can be found, in the online version, at doi:10.1016/j.epsl.2008.10.016.

References

Berner, R.A., 1981. A new geochemical classification of sedimentary environments. J. Sediment. Petrol. 51, 359–365.
Berner, R.A., 1984. Sedimentary pyrite formation — an update. Geochim. Cosmochim. Acta 48, 605–615.
Bloemendal, J., King, J.W., Hall, F.R., Doh, S.J., 1992. Rock magnetism of Late Neogene and Pleistocene deep-sea sediments: relationship to sediment source, diagenetic processes, and sediment lithology. J. Geophys. Res. 97, 4361–4375.
Bloemendal, J., King, J.W., Hunt, A., DeMenocal, P.B., Hayashida, A., 1993. Origin of the sedimentary magnetic record at Ocean Drilling Program sites on the Owen Ridge, western Arabian Sea. J. Geophys. Res. 98, 4199–4219.
Bottrell, S.H., Parkes, R.J., Cragg, B.A., Raiswell, R., 2000. Isotopic evidence for anoxic pyrite oxidation and stimulation of bacterial sulphate reduction in marine sediments. J. Geol. Soc. (Lond.) 157, 711–714.
Bryson, G., 2006. Quaternary monsoon variation in the north-west Arabian Sea from planktonic foraminifera assemblages. MSc thesis, School of Ocean and Earth Science, University of Southampton.
Canfield, D.E., Berner, R.A., 1987. Dissolution and pyritization of magnetite in anoxic marine sediments. Geochim. Cosmochim. Acta 51, 645–659.
Channell, J.E.T., Hawthorne, T., 1990. Progressive dissolution of titanomagnetites at ODP Site 653 (Tyrrhenian Sea). Earth Planet. Sci. Lett. 96, 469–480.
Day, R., Fuller, M., Schmidt, V.A., 1977. Hysteresis properties of titanomagnetites: grain size and composition dependence. Phys. Earth Planet. Inter. 13, 260–266.
Dean, W.E., Gardner, J.V., Anderson, R.Y., 1994. Geochemical evidence for enhanced preservation of organic matter in the oxygen minimum zone of the continental margin of northern California during the late Pleistocene. Paleoceanography 9, 47–61.
Dekkers, M.J., Langereis, C.G., Vriend, S.P., Van Santvoort, P.J.M., DeLange, G.J., 1994. Fuzzy c-means cluster analysis of early diagenetic effects on natural remanent magnetization acquisition in a 1.1 Myr piston core from the Central Mediterranean. Phys. Earth Planet. Inter. 85, 155–171.
Dillon, M., Bleil, U., 2006. Rock magnetic signatures in diagenetically altered sediments from the Niger deep-sea fan. J. Geophys. Res. 111 (B03105). doi:10.1029/2004JB003540.
Dunlop, D.J., 2002. Theory and application of the Day plot (M_{rs}/M_s versus H_{cr}/H_c) 1. Theoretical curves and tests using titanomagnetite data. J. Geophys. Res. 107 (B2056). doi:10.1029/2001JB000486.
Emiroglu, S., Rey, D., Petersen, N., 2004. Magnetic properties of sediment in the Ria de Arousa (Spain): dissolution of iron oxides and formation of iron sulphides. Phys. Chem. Earth 29, 947–959. doi:10.1016/j.pce.2004.03.012.
Florindo, F., Sagnotti, L., 1995. Palaeomagnetism and rock magnetism in the upper Pliocene Valle Ricca (Rome, Italy) section. Geophys. J. Int. 123, 340–354.
Gardner, J.V., Dean, W.E., Dartnell, P., 1997. Biogenic sedimentation beneath the California Current system for the past 30 kyr and its paleoceanographic significance. Paleoceanography 12, 207–225.
Garming, J.F.L., Bleil, U., Riedinger, N., 2005. Alteration of magnetic mineralogy at the sulfate–methane transition: analysis of sediments from the Argentine continental slope. Phys. Earth Planet. Inter. 151, 290–308. doi:10.1016/j.pepi.2005.04.001.
Harrison, R.J., Feinberg, J.M., 2008. FORCinel: an improved algorithm for calculating first-order reversal curve distributions using locally weighted regression smoothing. Geochem. Geophys. Geosyst. 9 (Q05016). doi:10.1029/2008GC001987.
Horng, C.S., Chen, J.C., Lee, T.Q., 1992. Variations in magnetic minerals from two Plio-Pleistocene marine-deposited sections, southwestern Taiwan. J. Geol. Soc. China 35, 323–335.
Horng, C.S., Torii, M., Shea, K.S., Kao, S.J., 1998. Inconsistent magnetic polarities between greigite- and pyrrhotite/magnetite-bearing marine sediments from the Tsailiaochi section, southwestern Taiwan. Earth Planet. Sci. Lett. 164, 467–481.
Hounslow, M.W., Maher, B.A., 1999. Source of the climate signal recorded by magnetic susceptibility variations in Indian Ocean sediments. J. Geophys. Res. 104, 5047–5061.
Hunger, S., Benning, L.G., 2007. Greigite: a true intermediate on the polysulfide pathway to pyrite. Geochem. Trans. 8 (1). doi:10.1186/1467-4866-8-1.
Jacobs, C.L., 2003. RRS Charles Darwin Cruise 143, 22 Nov–20 Dec 2002. SCHEHEREZADE II: Geological and biological surveys of the Arabian Sea and the continental slope of Oman. Vol. 79 of Southampton Oceanography Centre Cruise Report. Southampton, UK.
Jiang, W.T., Horng, C.S., Roberts, A.P., Peacor, D.R., 2001. Contradictory magnetic polarities in sediments and variable timing of neoformation of authigenic greigite. Earth Planet. Sci. Lett. 193, 1–12.
Jørgensen, B.B., Böttcher, M.E., Lüschen, H., Neretin, L.N., Volkov, I.I., 2004. Anaerobic methane oxidation and a deep H_2S sink generate isotopically heavy sulfides in Black Sea sediments. Geochim. Cosmochim. Acta 68, 2095–2118. doi:10.1016/j.gca.2003.07.017.
Kao, S.J., Horng, C.S., Roberts, A.P., Liu, K.K., 2004. Carbon–sulfur–iron relationships in sedimentary rocks from southwestern Taiwan: influence of geochemical environment on greigite and pyrrhotite formation. Chem. Geol. 203, 153–168. doi:10.1016/j.chemgeo.2003.09.007.

Karlin, R., 1990a. Magnetic mineral diagenesis in suboxic sediments at Bettis site W-N, NE Pacific Ocean. J. Geophys. Res. 95, 4421–4436.
Karlin, R., 1990b. Magnetite diagenesis in marine sediments from the Oregon continental margin. J. Geophys. Res. 95, 4405–4419.
Karlin, R., Levi, S., 1983. Diagenesis of magnetic minerals in recent haemipelagic sediments. Nature 303, 327–330.
Karlin, R., Levi, S., 1985. Geochemical and sedimentological control of the magnetic properties of hemipelagic sediments. J. Geophys. Res. 90, 373–392.
Kasten, S., Freudenthal, T., Gingele, F.X., Schulz, H.D., 1998. Simultaneous formation of iron-rich layers at different redox boundaries in sediments from the Amazon deep-sea fan. Geochim. Cosmochim. Acta 62, 2253–2264.
Larrasoaña, J.C., Roberts, A.P., Stoner, J.S., Richter, C., Wehausen, R., 2003. A new proxy for bottom-water ventilation in the eastern Mediterranean based on diagenetically controlled magnetic properties of sapropel-bearing sediments. Palaeogeogr. Palaeoclimatol. Palaeoecol. 190, 221–242. doi:10.1016/S0031-0182(02)00607-7.
Larrasoaña, J.C., Roberts, A.P., Musgrave, R.J., Gràcia, E., Piñero, E., Vega, M., Martinéz-Ruiz, F., 2007. Diagenetic formation of greigite and pyrrhotite in gas hydrate marine sedimentary systems. Earth Planet. Sci. Lett. 261, 350–366. doi:10.1016/j.epsl.2007.06.032.
Leslie, B.W., Hammond, D.E., Berelson, W.M., Lund, S.P., 1990a. Diagenesis in anoxic sediments from the California continental borderland and its influence on iron, sulfur, and magnetite behavior. J. Geophys. Res. 95, 4453–4470.
Leslie, B.W., Lund, S.P., Hammond, D.E., 1990b. Rock magnetic evidence for the dissolution and authigenic growth of magnetic minerals within anoxic marine sediments of the California continental borderland. J. Geophys. Res. 95, 4437–4452.
Liu, J., Zhu, R.X., Roberts, A.P., Li, S.Q., Chang, J.H., 2004. High-resolution analysis of early diagenetic effects on magnetic minerals in post-middle-Holocene continental shelf sediments from the Korea Strait. J. Geophys. Res. 109 (B03103). doi:10.1029/2003JB002813.
Nair, R.R., Ittekkot, V., Manganini, S.J., Ramaswany, V., Haake, B., Degens, E.T., Desai, B.N., Honjo, S., 1989. Increased particle flux to the deep ocean related to monsoons. Nature 338, 749–751.
Neretin, L.N., Böttcher, M.E., Jørgensen, B.B., Volkov, I.I., Lüschen, H., Hilgenfeldt, K., 2004. Pyritization processes and greigite formation in the advancing sulfidization front in the Upper Pleistocene sediments of the Black Sea. Geochim. Cosmochim. Acta 68, 2081–2093. doi:10.1016/S0016-7037(00)00450-2.
Pike, C.R., Roberts, A.P., Verosub, K.L., 1999. Characterizing interactions in fine magnetic particle systems using first order reversal curves. J. Appl. Phys. 85, 6660–6667.
Pike, C.R., Roberts, A.P., Verosub, K.L., 2001. First-order reversal curve diagrams and thermal relaxation effects in magnetic particles. Geophys. J. Int. 145, 721–730.
Raiswell, R., 1982. Pyrite texture, isotopic composition and the availability of iron. Am. J. Sci. 282, 1244–1263.
Rey, D., Mohamed, K.J., Bernabeu, A., Rubio, B., Vilas, F., 2005. Early diagenesis of magnetic minerals in marine transitional environments: geochemical signatures of hydrodynamic forcing. Mar. Geol. 215, 215–236. doi:10.1016/j.margeo.2004.12.001.
Riedinger, N., Pfeifer, K., Kasten, S., Garming, J.F.L., Vogt, C., Hensen, C., 2005. Diagenetic alteration of magnetic signals by anaerobic oxidation of methane related to a change in sedimentation rate. Geochim. Cosmochim. Acta 69, 4117–4126. doi:10.1016/j.gca.2005.02.004.
Roberts, A.P., 1995. Magnetic properties of sedimentary greigite (Fe_3S_4). Earth Planet. Sci. Lett. 134, 227–236.
Roberts, A.P., Turner, G.M., 1993. Diagenetic formation of ferrimagnetic iron sulphide minerals in rapidly deposited marine sediments, South Island, New Zealand. Earth Planet. Sci. Lett. 115, 257–273.
Roberts, A.P., Weaver, R., 2005. Multiple mechanisms of remagnetization involving sedimentary greigite (Fe_3S_4). Earth Planet. Sci. Lett. 231, 263–277. doi:10.1016/j.epsl.2004.11.024.
Roberts, A.P., Pike, C.R., Verosub, K.L., 2000. First-order reversal curve diagrams: a new tool for characterizing the magnetic properties of natural samples. J. Geophys. Res. 105, 28461–28475.
Roberts, A.P., Jiang, W.T., Florindo, F., Horng, C.S., Laj, C., 2005. Assessing the timing of greigite formation and the reliability of the upper Olduvai polarity transition record from the Crostolo River, Italy. Geophys. Res. Lett. 32 (L05307). doi:10.1029/2004GL022137.
Robinson, S.G., Sahota, J.T.S., Oldfield, F., 2000. Early diagenesis in North Atlantic abyssal plain sediments characterized by rock-magnetic and geochemical indices. Mar. Geol. 163, 77–107.
Rowan, C.J., Roberts, A.P., 2005. Tectonic and geochronological implications of variably timed magnetizations carried by authigenic greigite in marine sediments from New Zealand. Geology 33, 553–556. doi:10.1130/G21382.1.
Rowan, C.J., Roberts, A.P., 2006. Magnetite dissolution, diachronous greigite formation, and secondary magnetizations from pyrite oxidation: unravelling complex magnetizations in Neogene marine sediments from New Zealand. Earth Planet. Sci. Lett. 241, 119–137. doi:10.1016/j.epsl.2005.10.017.
Rowan, C.J., Roberts, A.P., 2008. Widespread remagnetizations and a new view of tectonic rotations within the Australia–Pacific plate boundary zone, New Zealand. J. Geophys. Res. 113 (B03103). doi:10.1029/2006JB004594.
Sagnotti, L., Winkler, A., 1999. Rock magnetism and palaeomagnetism of greigite-bearing mudstones in the Italian peninsula. Earth Planet. Sci. Lett. 165, 67–80.
Sagnotti, L., Roberts, A.P., Weaver, R., Verosub, K.L., Florindo, F., Pike, C.R., Clayton, T., Wilson, G.S., 2005. Apparent magnetic polarity reversals due to remagnetization resulting from late diagenetic growth of greigite from siderite. Geophys. J. Int. 160, 89–100. doi:10.1111/j.1365-246X.2005.02485.x.
Schwehr, K., Tauxe, L., Driscoll, N., Lee, H., 2006. Detecting compaction disequilibrium with anisotropy of magnetic susceptibility. Geochem. Geophys. Geosyst. 7 (Q11002). doi:10.1029/2006GC001378.
Sirocko, F., Garbe-Schönberg, D., Devey, C., 2000. Processes controlling trace element geochemistry of Arabian Sea sediments during the last 25,000 years. Glob. Planet. Change 26, 217–303.
Snowball, I.F., 1997. Gyroremanent magnetization and the magnetic properties of greigite-bearing clays in southern Sweden. Geophys. J. Int. 129, 624–636.
Tarduno, J.A., 1992. Magnetic susceptibility cyclicity and magnetic dissolution in Cretaceous limestones of the Southern Alps (Italy). Geophys. Res. Lett. 19, 1515–1518.
Tarduno, J.A., 1994. Temporal change of magnetite dissolution in the pelagic realm: gauging paleoproductivity? Earth Planet. Sci. Lett. 123, 39–48.
Tarduno, J.A., 1995. Superparamagnetism and reduction diagenesis in pelagic sediments — enhancement or depletion? Geophys. Res. Lett. 22, 1337–1340.
Tric, E., Laj, C., Jehanno, C., Valet, J.P., Kissel, C., Mazaud, A., Iaccarino, S., 1991. High-resolution record of the upper Olduvai transition from the Po Valley (Italy) sediments: support for dipolar transition geometry? Phys. Earth Planet. Inter. 65, 319–336.
Vasiliev, I., Dekkers, M.J., Krijgsman, W., Franke, C., Langereis, C.G., Mullender, T.A.T., 2007. Early diagenetic greigite as a recorder of the palaeomagnetic signal in Miocene–Pliocene sedimentary rocks of the Carpathian foredeep (Romania). Geophys. J. Int. 171, 613–629. doi:10.1111/j.1365-246X.2007.03560.x.
Weeks, R., Laj, C., Endignoux, L., Fuller, M., Roberts, A., Manganne, R., Blanchard, E., Goree, W., 1993. Improvements in long core measurement techniques: applications in palaeomagnetism and palaeoceanography. Geophys. J. Int. 114, 651–662.
Wilkin, R.T., Barnes, H.L., 1997. Formation processes of framboidal pyrite. Geochim. Cosmochim. Acta 61, 323–339.
Yamazaki, T., Abdeldayem, A.L., Ikehara, K., 2003. Rock-magnetic changes with reduction diagenesis in Japan Sea sediments and preservation of geomagnetic secular variation in inclination during the last 30,000 years. Earth Planets Space 55, 327–340.